J. Fluid Mech. (2002), *vol.* 473, *pp.* 379–388.
DOI: 10.1017/S0022112002002628 Printed in the United Kingdom

Shear versus vortex-induced lift force on a rigid sphere at moderate *Re*

By P. BAGCHI AND S. BALACHANDAR

Department of Theoretical and Applied Mechanics, University of Illinois at Urbana-Champaign, Urbana, IL 61801, USA

(Received 27 June 2002 and in revised form 20 August 2002)

The lift forces on rigid spheres entrained in a vortex and a linear shear flow are computed using a direct numerical simulation. The sphere Reynolds number is in the range 10 to 100. The lift coefficient in a vortex is shown to be nearly two orders of magnitude higher than that in a shear flow. The inviscid mechanism is shown to be inadequate to account for the enhanced lift force. The effect of free rotation of the sphere is also shown to be too small to account for the enhanced lift force. Flow structure around the sphere is studied to explain the generation of the strong lift force in a vortex.

1. Introduction

The lift force on spheres in rotational flows, such as shear flows and vortices, has been a subject of interest for many years. In a linear shear flow, for moderate values of Reynolds number in the range 10 to 100 and non-dimensional ambient vorticity below 0.1, the lift coefficient computed by Kurose & Komori (1999) and Bagchi & Balachandar (2002*a*) was generally very small, in the range −0.01 to 0.01. In particular, they observed the lift coefficient to become negative above a Reynolds number of about 50. In contrast, the measurements of Sridhar & Katz (1995) for the case of bubbles in a vortical flow, over the same Reynolds number range and non-dimensional ambient vorticity, showed an order of magnitude larger lift coefficient, in the range 0.1 to 0.3. The experiments considered contaminated bubbles, which behave like rigid spheres, entrained in a vortex. The measured lift force was always positive, directed away from the centre of the vortex and was observed to be independent of the Reynolds number.

In the inviscid limit, the lift force on a sphere in a linear shear flow is different from that in a vortex (ambient fluid in rigid body rotation) (Auton, Hunt & Prud'homme 1988). Under steady conditions the force on the sphere in the inviscid limit can be written as

$$\boldsymbol{F} = m_f(1 + C_M)\boldsymbol{u} \cdot \nabla \boldsymbol{u} + m_f C_{IL} \boldsymbol{u}_r \times \boldsymbol{\omega}, \tag{1.1}$$

where $\boldsymbol{u}_r = \boldsymbol{u} - \boldsymbol{v}$ is the slip velocity, $\boldsymbol{v}$ is the velocity of the sphere, $\boldsymbol{u}$ and $\boldsymbol{\omega}$ are the velocity and vorticity of the undisturbed ambient flow at the centre of the sphere and m_f is the mass of fluid displaced by the sphere. The coefficients C_M and C_{IL} are the added-mass and the inviscid lift coefficients, and for a sphere, the former is always 1/2, while the latter is 1/2 provided the vorticity and any unsteady effects are weak (Auton *et al.* 1988). The contribution from the second term on the right-hand side remains the same in a shear flow and in a vortex. The contribution from the first term for a shear flow is identically zero, while for a vortex its contribution is negative,

directed towards the centre of the vortex. Thus according to inviscid theory the lift force on a rigid sphere in a vortex is less than that in a linear shear flow.

In the creeping flow limit, neither a linear ambient shear nor an ambient solid body rotation influences the force on the sphere. At small but finite Reynolds number ($Re < 1$), the shear-induced lift force (Saffman 1965) and the lift force in a vortex (Herron, Davis & Bretherton 1975) are both positive (directed from the low-speed to the high-speed side of the sphere) and are proportional to the square root of the ambient vorticity. However, the lift force in a vortex is about 24% larger.

In view of the above predictions of the inviscid and low-Re theories, the substantially enhanced lift force in a vortex measured by Sridhar & Katz (1995) is intriguing. They suggested rotation of the sphere as a possible mechanism for the enhancement. Here we will perform well-resolved three-dimensional direct numerical simulations of a stationary rigid sphere in an ambient flow of solid body rotation. The results on the detailed flow field and forces on the sphere will be compared to those for a sphere subjected to a linear shear flow. The range of sphere Reynolds number considered here is 10 to 100 and the dimensionless ambient vorticity will be varied up to 0.1. It is of particular interest to see if the sphere experiences a substantially enhanced lift force in the case of a vortex. The viscous and pressure contributions will be separated to highlight the role of the no-slip condition. In addition to the stationary sphere, we will also perform direct numerical simulations of a rigid sphere in a vortex, which is allowed to freely rotate in response to the hydrodynamic torque acting on it. These simulations will illustrate the effect of sphere rotation on the wake structure and on the lift and drag forces. It must be emphasized that the present simulations do not reproduce the precise experimental conditions of Sridhar & Katz (1995) – the ambient flow is an idealized solid body rotation and the sphere is held fixed and not allowed to translate. Therefore comparison with their results is only qualitative.

2. Methodology

We employ a direct numerical simulation (DNS) technique using a high-resolution pseudospectral method to study the flow past a sphere. The ambient linear shear and vortex flows are given by

$$\text{shear:} \quad U_X = |\boldsymbol{u}_r|\boldsymbol{e}_X + \omega Y, \quad U_Y = 0, \quad U_Z = 0, \tag{2.1}$$

$$\text{vortex:} \quad U_X = |\boldsymbol{u}_r|\boldsymbol{e}_X + \tfrac{1}{2}\omega Y, \quad U_Y = -\tfrac{1}{2}\omega X, \quad U_Z = 0, \tag{2.2}$$

where X, Y, Z represents a fixed reference frame. The centre of the sphere of diameter d is located at the centre of this frame. The relative velocity measured at the centre of the sphere is $\boldsymbol{u}_r$, and it is directed towards the positive X-axis. The dimensionless vorticity ω^* is in the range 0.04 to 0.1 and the Reynolds number Re is in the range 10 to 100, which are chosen to match the experimental condition of Sridhar & Katz (1995).

The DNS scheme used in this study employs a Fourier–Chebyshev collocation scheme for spatial discretization, and a two-step time-split scheme for time advancing. The governing equations (continuity and momentum) are solved in a spherical domain ($d/2 \leqslant r \leqslant D/2$, $0 \leqslant \theta \leqslant \pi$, $0 \leqslant \phi \leqslant 2\pi$) of outer boundary D that is 30 times the diameter of the sphere. At the inflow section of the domain, the undisturbed ambient flow given by (2.1) or (2.2) is specified. At the outflow section, a non-reflecting boundary condition is employed by parabolizing the governing equations. On the surface of the sphere, the no-penetration and no-slip conditions are satisfied. A typical

		Sridhar & Katz	Kurose & Komori	Present results	
Re	$\omega d/\lvert\boldsymbol{u}_r\rvert$	Vortex	Shear	Vortex	Shear
25	0.04	0.182* (0.15–0.3)†	0.001	0.181	0.005
50	0.04	0.182* (0.15–0.3)†	−0.001	0.137	0.001
100	0.04	0.182* (0.15–0.3)†	−0.004	0.097	−0.003
50	0.1	0.179* (0.1–0.25)†	−0.002	0.347	0.001
100	0.1	0.179* (0.1–0.25)†	−0.008	0.237	−0.008

TABLE 1. Lift coefficients on a rigid sphere in vortex and shear flows. * Based on $0.5(\omega^*)^{0.25}$; † based on the data given in Sridhar & Katz (1995).

grid used in the present computation has 111 points in the radial direction, 112 points in the tangential direction and 48 points in the azimuthal direction. The resultant force on the sphere is computed by integrating the pressure and viscous stresses on the surface of the sphere. Further details on the methodology and implementation are given in Bagchi & Balachandar (2002*b*).

3. Results

3.1. *Lift and drag forces*

The lift coefficients defined as

$$C_L = \frac{F_Y}{\frac{1}{2}\pi\rho_f|\boldsymbol{u}_r|^2(\frac{1}{2}d)^2}, \tag{3.1}$$

computed from the present simulations for the shear and vortex flows are shown in table 1. In the above equation F_Y is the dimensional force along the Y-direction, and ρ_f is the density of the fluid. The lift coefficients measured by Sridhar & Katz (1995) for the case of bubbles in a vortex are also shown: both the range of C_L estimated from their data, and the values obtained from the curve fit $0.5(\omega^*)^{0.25}$ are shown ($\omega^* = \omega d/|\boldsymbol{u}_r|$ is the non-dimensional vorticity). In the case of linear shear flow the lift coefficients are very small and decrease with increasing *Re* and become negative for Reynolds number greater than about 50, which is consistent with the results of Kurose & Komori (1999). The computed lift coefficients for a stationary sphere in a vortex are more than an order of magnitude larger and for all the cases considered remain positive.

The DNS results for the vortex are only in qualitative agreement with the experimental results of Sridhar & Katz (1995): they both show substantially enhanced lift when compared to the corresponding linear shear flow at the same *Re* and ω^*. The idealized solid body rotation for the undisturbed ambient flow considered in the present simulations is only a crude approximation to the experimentally generated vortex ring. In the experiments the bubble is allowed to freely move and the resulting slip velocity between the bubble and the surrounding flow is likely to have both radial and circumferential components. In the computations, by considering a stationary sphere the slip velocity has been constrained to be purely circumferential. Other differences could arise from the unavoidable experimental uncertainties in tracking bubble location, size and sphericity. Such differences contribute to the quantitative disagreement between the computed and experimental results.

Figure 1 shows the variation of the lift force with *Re* and ω^* for both the linear shear and vortex flows. The corresponding inviscid predictions, which are also plotted

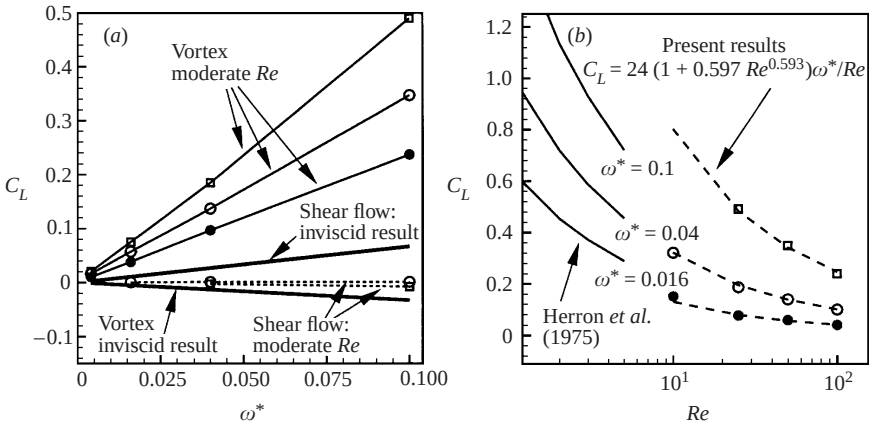

FIGURE 1. Variation of the lift forces with Re and ω^*. (a) Thick lines are inviscid results; ●, $Re = 100$; ○, $Re = 50$; □, $Re = 25$. (b) ●, $\omega^* = 0.016$; ○, $\omega^* = 0.04$; □, $\omega^* = 0.1$.

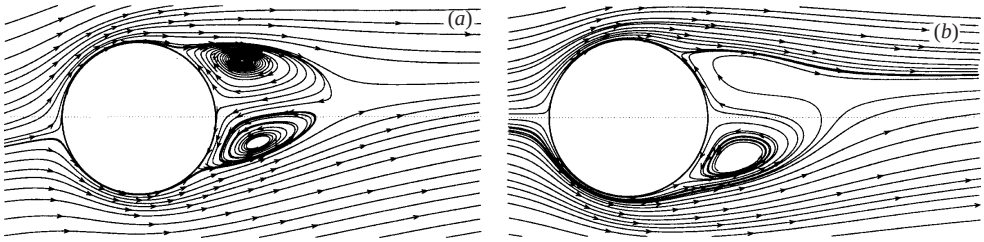

FIGURE 2. Streamlines for the fixed spheres at $Re = 100$, $\omega^* = 0.1$ in (a) vortex flow and (b) linear shear flow. The dashed line indicates the centreplane.

in the figure, show that for both the linear shear and vortex flows the actual lift force is oriented in the opposite direction. The lift coefficient for the vortex case shows a near linear increase with the ambient vorticity. In contrast to the experimental results of Sridhar & Katz (1995), figure 1(b) shows a clear monotonic decrease in C_L with increasing Re. Over the range of parameters considered a good fit of the DNS data can be obtained as

$$C_L = \frac{24}{Re}[1 + 0.597Re^{0.593}]\omega^*. \tag{3.2}$$

In comparison, over the range of Re and ω^* considered the drag force remains insensitive to ambient shear and solid body rotation.

Figure 2 compares the streamlines for the linear shear and vortex flows at $Re = 100$ and $\omega^* = 0.1$. At this Re the flow is steady and the (X, Y)-plane ($Z = 0$) is a plane of symmetry, on which the out-of-plane velocity is identically zero; in figure 2 the streamlines correspond to the in-plane velocity. Clearly both the ambient shear and pure rotation break the axisymmetry about the X-axis, which one would otherwise observe for a uniform cross-flow. However, the structure of the wake flow is significantly different in the vortex and shear flow cases. In the vortex flow, the front stagnation point is located slightly below the centreplane ($Y = 0$), and the rear stagnation point is pushed up above the centreplane. In the shear flow, however, the stagnation points are located on the centreplane.

The lift coefficient can be decomposed into the pressure and shear stress contributions. Note that the normal viscous stress on the surface of the sphere is identically

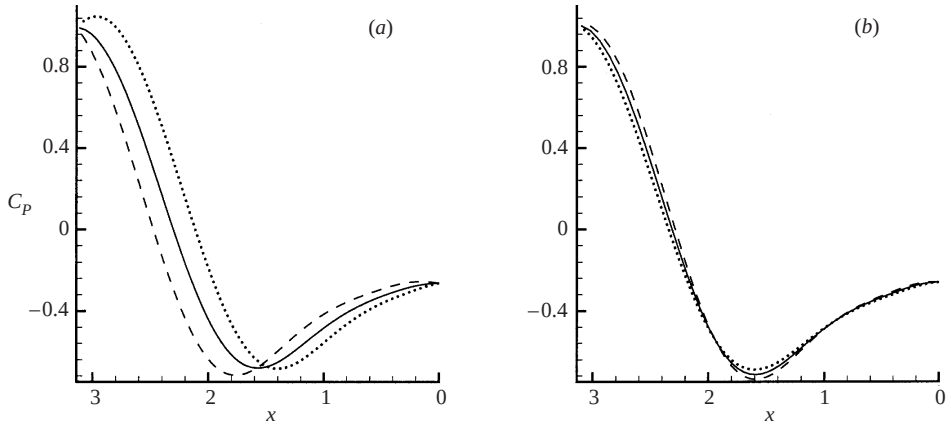

FIGURE 3. Surface pressure coefficients for the fixed spheres at $Re = 100$, $\omega^* = 0.1$ in (a) vortex flow and (b) linear shear flow. ——, C_P averaged over the azimuthal direction ϕ from 0 to 2π; - - - - -, C_P along $\phi = 0$ (top surface); · · · · · ·, C_P along $\phi = \pi$ (bottom surface).

zero, and hence does not contribute to the drag or lift forces. The pressure and shear stresses are made dimensionless by $\rho_f|\boldsymbol{u}_r|^2$. The pressure contribution in terms of the surface pressure coefficient C_P is shown in figure 3. We consider the variation of C_P with the tangential direction θ along $\phi = 0$ and $\phi = \pi$, where C_P has extremum values. Here θ increases from 0 to π from the rear to the front of the sphere, and $\phi = 0$ and $\phi = \pi$ correspond to the top and bottom meridional lines. The ϕ-averaged C_P, defined as $\langle C_P \rangle = (1/2\pi)\int_0^{2\pi} C_P \, \mathrm{d}\phi$ is also shown. Consider first the vortex flow. On the windward side of the sphere ($\theta > \pi/2$), a higher-than-average pressure is generated over the bottom surface, while a lower-than-average pressure is generated over the top surface. As a result, a strong upward (or, positive) Y force is generated on the windward side. On the leeward side ($\theta < \pi/2$), a higher-than-average pressure exists over the top surface, and a lower-than-average pressure exists over the bottom surface. Thus a negative force is generated on the leeward side. However, due to the presence of the wake, the pressure is not fully recovered on the leeward side. Therefore the positive contribution coming from the windward side outweighs the negative contribution from the leeward side, making the net pressure contribution positive. Consider next the case of a shear flow. The windward side now makes a negative contribution. Some positive contribution exists near $\theta = \pi/2$. The integrated effect is a very small lift force, which is positive at low Re, and negative at higher Re.

The shear stress contribution to the lift force is shown in figure 4 in terms of surface contours of $(\tau_{r\theta}\boldsymbol{e}_\theta + \tau_{r\phi}\boldsymbol{e}_\phi)\cdot\boldsymbol{e}_Y$. A positive contour indicates a local positive contribution to lift. In the case of a vortex, the stronger shear on the upper front quadrant of the sphere contributes positively to the lift force, and outweighs the negative contribution arising from the somewhat weaker shear over the bottom quadrant. In the shear flow, the positive and negative contributions nearly balance each other. In both the vortex and the shear flow, very little contribution to the pressure and viscous components of the lift force comes from the wake region, thus emphasizing the effect of no slip and the presence of a recirculation region and the associated lack of pressure recovery. In both cases the shear stresses contribute about 50% to 60% of the total lift force.

The force coefficient, $\boldsymbol{C}_F = C_D\boldsymbol{e}_x + C_L\boldsymbol{e}_y$, for the present case of a stationary sphere in a steady ambient flow, can be written as

$$\boldsymbol{C}_F = \tfrac{4}{3}(1 + C_M)\boldsymbol{u}^* \cdot \nabla\boldsymbol{u}^* + \tfrac{4}{3}C_{IL}\hat{\boldsymbol{u}}_r \times \boldsymbol{\omega}^* + \boldsymbol{C}_{sv}, \tag{3.3}$$

		Pressure gradient and added-mass		Inviscid rotational		Steady viscous lift	
Re	$\omega d/\lvert\boldsymbol{u}_r\rvert$	Vortex	Shear	Vortex	Shear	Vortex	Shear
25	0.04	−0.04	0.0	0.027	0.027	0.194	−0.022
50	0.04	−0.04	0.0	0.027	0.027	0.150	−0.026
100	0.04	−0.04	0.0	0.027	0.027	0.110	−0.030
50	0.1	−0.1	0.0	0.067	0.067	0.380	−0.066
100	0.1	−0.1	0.0	0.067	0.067	0.270	−0.075

TABLE 2. The dimensionless contributions to the lift force from different terms in (3.3).

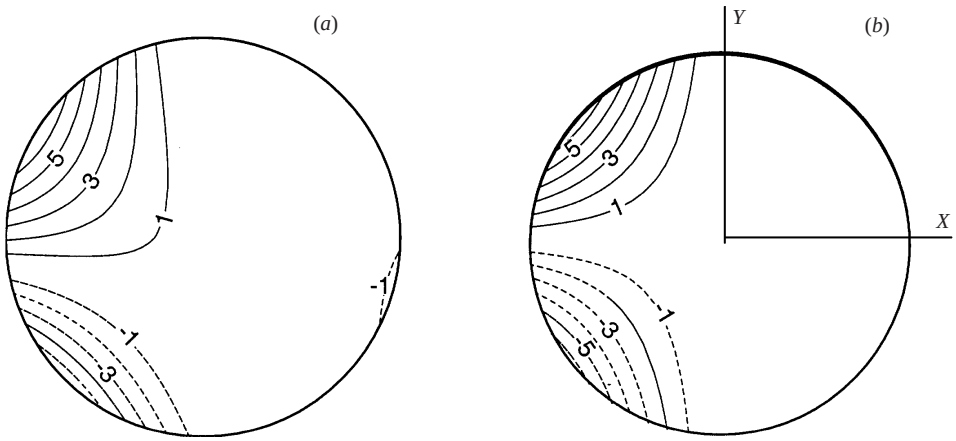

FIGURE 4. Contours of the Y-component of the shear stress on the surface of the sphere: (a) vortex flow, (b) shear flow. Because of symmetry, only one half of the sphere is shown. The contours are plotted in steps of 1.0. The dashed lines indicate negative values. The flow is from left to right. The view shown here is looking towards the negative Z-axis.

where $\hat{\boldsymbol{u}}_r$ is the unit vector along $\boldsymbol{u}_r$, and the symbol * is used to denote dimensionless quantities ($|\boldsymbol{u}_r|$ and d are used as the velocity and length scales). In the above equation all the fluid quantities ($\boldsymbol{u}^* \cdot \nabla \boldsymbol{u}^*$, $\boldsymbol{\omega}^*$) are of the undisturbed ambient flow evaluated at the centre of the sphere. At moderate Re, in addition to the inviscid forces represented by the first two terms on the right, the steady viscous effect $\boldsymbol{C}_{sv}$ also makes an additional contribution to the force. With $C_M = C_{IL} = 1/2$, the inviscid forces are known and therefore $\boldsymbol{C}_{sv}$ can be extracted from the computed total force. The lift component of $\boldsymbol{C}_{sv}$ is shown in table 2 along with the inviscid forces for both the shear and vortex. The added-mass and pressure gradient forces (first term on the right) contribute negatively for the vortex, whereas they are zero for the shear flow. The inviscid lift force, which depends only on the vorticity magnitude, is the same in both the vortex and the shear flow. It is always positive, i.e. directed outward from the centre of the vortex. The steady viscous force, on the other hand, is significantly different for the two cases. In a vortex, it is several times larger than the inviscid forces. As a result, a strong radially outward lift is generated for the case of a vortex. In the case of a shear flow, the steady viscous contribution remains comparable to the inviscid lift force. Thus the net lift force is small in a shear flow, and its sign changes from positive to negative with increasing Re.

3.2. *Free motion in a vortex*

Here we consider the effect of the high values of the lift force on the motion of a sphere in a vortex, as in the experiments of Sridhar & Katz (1995). For a sphere located at a distance r from the centre of the vortex, the equation of radial motion in cylindrical polar (r, γ, z) coordinates is

$$(\rho + \tfrac{1}{2})\frac{\partial v_r}{\partial t} = (\rho + \tfrac{1}{2})\frac{v_\gamma^2}{r} - \frac{3}{2}\frac{u_\gamma^2}{r} + \tfrac{1}{2}(1+f)(\boldsymbol{u}-\boldsymbol{v})\times\boldsymbol{\omega} - C_D\left(\frac{3}{4d}\right)|\boldsymbol{u}-\boldsymbol{v}|v_r, \quad (3.4)$$

where $\rho = \rho_p/\rho_f$ is the sphere-to-fluid density ratio. The quantity f provides the relative measure of the steady viscous lift force compared to the inviscid lift, and is given by

$$\boldsymbol{C}_{sv}\cdot\boldsymbol{e}_y = \tfrac{4}{3}C_{IL}f\hat{\boldsymbol{u}}_r\times\boldsymbol{\omega}^*. \quad (3.5)$$

The values of f can be obtained from the lift coefficients in table 2. In the inviscid limit $f = 0$, while over the moderate *Re* considered here it ranges from about 4 to 15. Consider a sufficiently small sphere, whose circumferential slip velocity to the leading order can be expressed as (Ferry & Balachandar 2001)

$$u_\gamma - v_\gamma \approx \epsilon u_\gamma, \quad (3.6)$$

where the constant $\epsilon = \frac{1}{2}\tau^2|\boldsymbol{\omega}|^2$, can be interpreted as the square of the ratio of particle time scale, τ, to the vortex time scale, $1/|\boldsymbol{\omega}|$. The above leading-order approximation for the circumferential slip becomes increasingly accurate for small ϵ. From (3.4) the radial acceleration is given by

$$\frac{u_\gamma^2}{r}\left[(1-\epsilon)^2 - \frac{3}{(2\rho+1)} + \frac{2\epsilon(1+f)}{(2\rho+1)}\right] - C_D\frac{3|\boldsymbol{u}-\boldsymbol{v}|v_r}{2d(2\rho+1)}. \quad (3.7)$$

The first term within the square brackets accounts for the centrifugal force arising from the circumferential motion of the sphere and the second term accounts for the pressure gradient and added-mass forces arising from hydrodynamic interaction with the surrounding fluid. These inertial effects account for the familiar radial outward migration of heavier-than-fluid particles ($\rho > 1$) and inward migration of lighter-than-fluid bubbles ($\rho < 1$). The radial component of the drag force is directed such that it opposes any radial motion of the sphere. The interest here is in the effect of the lift force which appears as the third term within the square bracket. This term accounts for both the inertial and steady viscous components of the lift force and is proportional to the circumferential slip velocity (i.e. linear in ϵ). The lift force will have a negligible effect on the radial motion of very heavy particles ($\rho \gg 1$). The lift force can however have a strong influence on the radial migration of lighter-than-fluid particles and bubbles. The present results show that the total lift force, due to the steady viscous contribution, can be significantly larger than the inertial lift. The effect of the lift force is to slow down the radial inward migration of bubbles, and such slowing down in the bubble entrainment process has been observed by Sridhar & Katz (1995). In fact, surprisingly, under the right conditions, it is possible for a bubble to migrate radially outward when the lift force begins to dominate the pressure gradient and added-mass forces.

3.3. *Sphere rotation*

We now consider the effect of sphere rotation. The viscous stresses over the surface of the sphere generate a hydrodynamic torque, which results in the angular acceleration

Re	$\omega d/\lvert\boldsymbol{u}_r\rvert$	C_L	Magnus lift	$\Omega_p d/\lvert\boldsymbol{u}_r\rvert$
25	0.04	0.189	0.008 (4%)	0.017
50	0.04	0.146	0.009 (6%)	0.017
100	0.04	0.113	0.016 (14%)	0.017
50	0.1	0.403	0.056 (14%)	0.037
100	0.1	0.255	0.018 (7%)	0.040

TABLE 3. Lift coefficients for a freely rotating rigid sphere in vortex. The Magnus lift is computed by the difference between the total lift forces on stationary and freely rotating spheres. The values in brackets indicate percentage of the total lift.

of the sphere. Under a steady ambient condition, the sphere will reach a terminal angular velocity at which the net torque on it is zero. Sridhar & Katz (1995) conjectured that the free rotation of the bubbles in their experiments was possibly responsible for the enhanced lift force in vortex. In order to address this issue, we have also simulated the flow past a stationary but freely rotating sphere in a vortex. In this case, in addition to the fluid flow equations, an angular momentum equation,

$$\boldsymbol{T} = I\frac{\mathrm{d}\boldsymbol{\Omega}_p}{\mathrm{d}t}, \tag{3.8}$$

is also solved for the rotational motion of the sphere, which provides the slip boundary condition on the surface of the sphere. $\boldsymbol{T}$ is the hydrodynamic torque on the sphere evaluated by integrating the shear stresses, I is the moment of inertia, and Ω_p is the sphere rotation rate. The sphere is allowed to rotate freely and reach a steady state. The lift coefficient under this torque-free steady condition is presented in table 3 and can be compared with that for a non-rotating sphere. Two different sphere-to-fluid density ratios, $\rho = 1.5$ and 5, were considered, which affected only the transient, and the final steady state was independent of ρ. The free rotation of the sphere contributes to an increase in the lift force due to the Magnus effect. However, its contribution is only 4%–14% of the total lift and can be considered to be only of secondary importance. In the case of shear flow as well, the effect of free rotation was observed to be quite weak (Bagchi & Balachandar 2002*a*).

The terminal rotation rate Ω_p of the sphere is also shown in the table. When scaled by the ambient rotation rate, the particle rotation rate is in the range 0.37 to 0.43, and nearly independent of Re and ω^*. It has been established in a shear flow that only in the Stokes limit does the sphere rotate at the same rate as the ambient flow and that as Re increases the terminal rotation rate of the sphere decreases (Poe & Acrivos 1975; Lin, Perry & Schowalter 1970; Ding & Aidun 2000; Patankar *et al.* 2001; Bagchi & Balachandar 2002*a*). For example, over the parameter range under consideration, in a shear flow the rotation rate of the sphere ranges from about 40% to 70% of ambient rotation rate. The flow structure around a freely rotating sphere in a vortex is shown in figure 5. No significant difference can be observed with the case of the non-rotating sphere shown in figure 2(*a*). Indeed, for a freely rotating sphere, a region of free streamline flow is expected to exist near the surface. But in the range of Re and vortex strength considered here, this region is extremely narrow (not visible up to the plotting accuracy). Thus the wake generated by the translational slip is far more important than the influence of any rotational slip between the sphere and the surrounding flow.

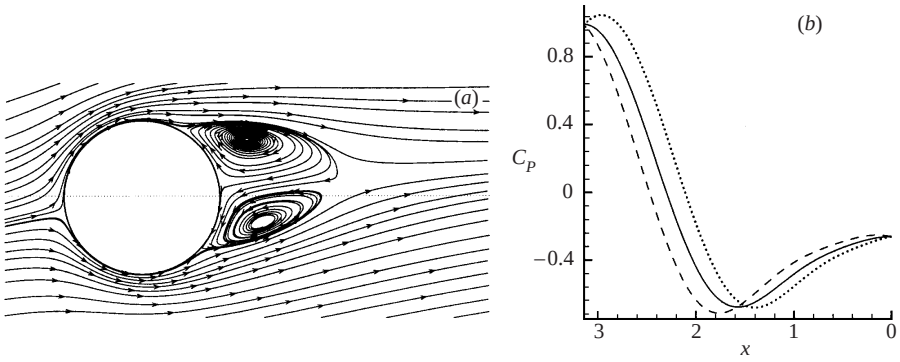

FIGURE 5. Free sphere in a vortex at $Re = 100$, $\omega^* = 0.1$. (*a*) Streamlines on $Z = 0$ plane, (*b*) surface pressure coefficients. ——, C_P averaged over ϕ; - - - - -, C_P along $\phi = 0$; · · · · · ·, C_P along $\phi = \pi$.

4. Conclusion

The purpose of this paper is to consider the problem of a rigid sphere in an otherwise undisturbed ambient flow of solid body rotation and quantitatively compare the results with the corresponding situation of a sphere in a linear shear flow of the same ambient vorticity magnitude. The difference between the two cases is clearly the presence of an ambient straining motion, in addition to vorticity, in the case of the linear shear flow. Analytical results for the above two cases, in both the inviscid and low-*Re* limits are available (Auton *et al.* 1988; Saffman 1965; Herron *et al.* 1975). Here the interest is in moderate Reynolds numbers ($Re \sim 10$–100), and dimensionless vorticity up to 0.1, and we employ direct numerical simulation. The lift coefficient in a vortex is shown to be nearly two orders of magnitude higher than that in a shear flow. The significantly enhanced lift force at moderate *Re* is in contrast to the results of the inviscid and low-*Re* theories. The viscous part of the lift force is isolated from the DNS results, and is shown to have opposite signs in the vortex and shear flows. The effect of the two different ambient flows on the detailed flow field around the body, in particular in the wake region, and the impact on the generation of lift force is studied. The effect of the strong positive viscous lift, which originates from a circumferential slip, on the radial migration of the sphere in a vortex is discussed. Additional DNS have been performed for a sphere allowed to freely rotate in response to hydrodynamic torque acting on it. A comparison of the results for the rotating and non-rotating spheres shows that the effect of free rotation is only secondary and cannot account for the enhanced lift in vortex.

The above results are qualitatively supported by the experimental results of Sridhar & Katz (1995), who measured substantially enhanced lift force for contaminated spherical bubbles entrained in a vortex. Their lift forces were also more than an order of magnitude larger than the corresponding values in a linear shear flow. The present simulations, however, do not duplicate their experimental condition and therefore quantitative differences exist between the present computational and the experimental results. For the case of a clean bubble (which satisfies a stress-free condition on its surface as opposed to no-slip), recent studies by Magnaudet & Legendre (1998) and Legendre & Magnaudet (1998) show that at larger Reynolds numbers the behaviour in both the shear flow and the vortex is captured well by the inviscid theory. The present DNS results and the measurements of Sridhar & Katz (1995) are markedly different from these results on clean bubbles, and hence they

emphasize the role of the no-slip boundary condition in the generation of the lift force.

This work is supported by the DOE ASCI Center for Simulation of Advanced Rockets at the University of Illinois at Urbana-Champaign. Computations are performed at the National Center for Supercomputing Applications at UIUC.

REFERENCES

Auton, T. R., Hunt, J. C. R. & Prud'homme, M. 1988 The force exerted on a body in inviscid unsteady non-uniform rotational flow. *J. Fluid Mech.* **197**, 241–257.

Bagchi, P. & Balachandar, S. 2002*a* Effect of free rotation on the motion of a solid sphere in linear shear flow at moderate *Re*. *Phys. Fluids* **14**, 2719–2737.

Bagchi, P. & Balachandar, S. 2002*b* Steady planar straining flow past a rigid sphere at moderate Reynolds number. *J. Fluid Mech.* **466**, 365–407.

Ding, E. J. & Aidun, C. K. 2000 The dynamics and scaling law for particles suspended in shear flow with inertia. *J. Fluid Mech.* **423**, 317–344.

Ferry, J. P. & Balachandar, S. 2001 A fast Eulerian method for dispersed two-phase flow. *Intl J. Multiphase Flow* **27**, 1199–1226.

Gotoh, I. 1990 Brownian motion in a rotating flow. *J. Statist. Phys.* **59**, 371–402.

Herron, I. H., Davis, S. H. & Bretherton, F. P. 1975 On the sedimentation of a sphere in a centrifuge. *J. Fluid Mech.* **68**, 209–234.

Kurose, R. & Komori, S. 1999 Drag and lift forces on a rotating sphere in a linear shear flow. *J. Fluid Mech.* **384**, 183–206.

Legendre, D. & Magnaudet, J. 1998 The lift force on a spherical bubble in a viscous linear shear flow. *J. Fluid Mech.* **368**, 81–126.

Lin, C. J., Peery, J. H. & Schowalter, W. R. 1970 Simple shear flow round a rigid sphere: inertial effects and suspension rheology. *J. Fluid Mech.* **44**, 1–17.

Magnaudet, J. & Legendre, I. 1998 Some aspects of the lift force on a spherical bubble. *Appl. Sci. Res.* **58**, 441–461.

McLaughlin, J. B. 1991 Inertial migration a small sphere in linear shear flows. *J. Fluid Mech.* **224**, 261–274.

Patankar, N. A., Huang, P. Y., Ko, T. & Joseph, D. D. 2001 Lift-off of a single particle in Newtonian and viscoelastic fluids by direct numerical simulation. *J. Fluid Mech.* **438**, 67–100.

Poe, G. G. & Acrivos, A. 1975 Closed-streamline flows past rotating single cylinders and spheres: inertia effects. *J. Fluid Mech.* **72**, 605–623.

Saffman, P. G. 1965 The lift on a small sphere in a slow shear flow. *J. Fluid Mech.* **22**, 385–400 (and Corrigendum, 1968, **31**, 624).

Sridhar, G. & Katz, J. 1995 Drag and lift forces on microscopic bubbles entrained by a vortex. *Phys. Fluids* **7**, 389–399.